ISSN 0915-633X

NATIONAL INSTITUTE FOR FUSION SCIENCE

Effects of Electric Field on Particle Drift Orbits in a $l = 2$ Torsatron

H. Sanuki, T. Kamimura, K. Hanatani, K. Itoh and J. Todoroki

(Received – Apr. 24, 1990)

NIFS-31

May 1990

RESEARCH REPORT
NIFS Series

NAGOYA, JAPAN

Effects of Electric Field on Particle Drift Orbits in a $l = 2$ Torsatron

H. Sanuki, T. Kamimura, K. Hanatani*,

K. Itoh and J. Todoroki

National Institute for Fusion Science,

Furocho, Chikusaku,

Nagoya, 464-01, Japan

* Plasma Physics Laboratory, Kyoto University,

Gokasho, Uji 611, Japan.

ABSTRACT

Particle orbits and loss regions in both real and velocity spaces are studied on the basis of the guiding center drift equations in magnetic coordinates. The boundary of loss region in pitch angle-radius ($\chi-\rho$) plane is determined from the condition whether the drift surfaces for helically trapped and transition particles reach the outermost magnetic surface or not. The loss boundaries for the absolute particle confinement, within of which boundary no particles are lost, is evaluated. Effects of the radial electric field, E_r on drift orbits and loss regions are discussed in detail. When ion motion is considered, the poloidal rotation modified by a positive E_r reduces a number of trapped particles and consequently it leads the improvement of particle confinement. For a small negative E_r, there is a possible particle loss caused by the helical resonance. The loss rate of ions caused by loss cone in collisionless limit is evaluated in the presence of E_r. Effect of ripple modulation on the loss region is also discussed briefly.

Key words: Drift equations,torsatrons,numerical calculations,
particle orbits,loss regions,ripple modulation,
radial electric field

I Introduction

The torsatron configurations with low to moderate aspect ratios have recently been attention with the advantage of a compact size and a high - beta operation. In these configurations, however, the distortion of magnetic surfaces caused by the toroidal perturbation is generally large and drives the radial drift of helically trapped particles, which enhances the collisionless particle losses. Since the large loss region in core plasma region is harmful to efficient heating and high energy particle confinement, the minimization of loss region is one of the important issues in compact torsatron configurations. Effects of the various types of modulations of helical field (HF) and the control of poloidal fields (PF) such as vertical and quadrupole field components are discussed associated with the improvement of particle confinement at design stage of a large helical device (LHD) [1–3]. It has also been pointed out theoretically that the presence of radial electric field can prevent the loss of helically trapped particles through $E \times B$ poloidal orbit rotation [4–6]. Generation of the radial electric field E_r has been observed in Wendelstein VII-A(W 7-A)[7] and Heliotron -E (H-E)[8] experiments and recently, the poloidal rotation profile is also measured and its electric field is spatially resolved by using emission spectroscopy technique in Compact Helical System (CHS) device [9].

The analytic formula [10,11] and the numerical analysis [12] based on the theory of J-invariant have been discussed to evaluate the loss region in both velocity and real spaces in the presence of the radial electric field. In Refs.[10] through [12], the minimum energy of particles entering the loss cone and an analytical expression have been obtained. However, we note that this evaluation of the minimum energy gives the upper bound because the transition particles with a smaller pitch angle may enter more easily into the loss cone. If the deviation of very energetic particle orbit from a magnetic surface

is large, the analytic treatment becomes intractable.

The purpose of this paper is to investigate the effect of radial electric field on the drift orbits of particles with an arbitary pitch angle and also its influence on the loss regions in the velocity space as well as in the real space, using a model magnetic field but by solving the guiding center drift equations in magnetic coordinates.

In Sec.II, the drift equations in magnetic coordinates are described. Drift orbits and loss regions in both real and velocity spaces for two cases without and with the radial electric field are studied in Sec.III. The minimum energy of trapped particles entering the loss region is also discussed in this section. Simple evaluation of loss rate caused by the loss cone is given in Sec.IV. The last section is devoted to the summary and discussions, which includes a brief consideration on the effect of ripple modulation.

II Drift Equations in Magnetic Coordinates

Following particle orbits in magnetic coordinates has the computational advantage of requiring only information about the magnitude of magnetic field B, not its vector components. Although the orbit equations in magnetic coordinates are derived for both vacuum and finite-bata fields [6], they are the simplest for a curl-free field. In this paper, we use the magnetic coordinates (ψ, θ, ϕ). The orientation of the coordinate system is shown in Fig.1. We apply the following collisionless guiding center drift equations in magnetic coordinates (ψ, θ, ϕ)[6];

$$\frac{d\psi}{dt} = -(\mu + B\rho_{\parallel}^2)\frac{\partial B}{\partial \theta}, \tag{1}$$

$$\frac{d\theta}{dt} = \frac{\partial \Phi}{\partial \psi} + (\mu + B\rho_{\parallel}^2)\frac{\partial B}{\partial \psi} + \iota B^2 \rho_{\parallel}/\hat{g}, \tag{2}$$

$$\frac{d\phi}{dt} = B^2 \rho_{\parallel}/\hat{g}, \tag{3}$$

$$\frac{d\rho_{\parallel}}{dt} = -(\mu + B\rho_{\parallel}^2)(\iota\frac{\partial B}{\partial \theta} + \frac{\partial B}{\partial \phi})/\hat{g}. \tag{4}$$

Here we choose a model magnetic field as

$$B(\psi,\theta,\phi) = 1 - \epsilon_t(\psi)\cos\theta + \epsilon_1(\psi,\theta)\cos(l\theta - M\phi), \tag{5}$$

with

$$\epsilon_t(\psi) = \epsilon_a(2\psi)^{1/2}, \tag{6}$$

$$\begin{aligned}\epsilon_1(\psi,\theta) &= \{[\epsilon_h - (\epsilon_h^{(-1)} + \epsilon_h^{(+1)})\cos\theta]^2 \\ &+ [(\epsilon_h^{(-1)} - \epsilon_h^{(+1)})\sin\theta]^2\}^{1/2},\end{aligned} \tag{7}$$

where particularly, for $l = 2$ torsatrons under consideration, we can take the forms of $\epsilon_h, \epsilon_h^{(-1)}$ and $\epsilon_h^{(+1)}$ as [13,14]

$$\epsilon_h = \epsilon_{ha}(2\psi), \tag{8}$$

$$\epsilon_h^{(-1)} = \delta_h^{(-1)}\epsilon_a(2\psi)^{1/2}, \tag{9}$$

$$\epsilon_h^{(+1)} = \delta_h^{(+1)}\epsilon_a(2\psi)^{3/2}. \tag{10}$$

In these equations, $\mu B = mv_\perp^2/2, \rho_\parallel = v_\parallel mc/eB$($v_\parallel$ is the parallel component of the velocity), Φ is an electrostatic potential, ι is the rotational transform, $\hat{g} = \epsilon_a^{-1}$ with $\epsilon_a = a/R_0$ (a is the plasma radius and R_0 is the major radius), and all quantities are mormalized in the same manner used in Ref.[15]. For example, the flux $\psi(= B_0 r^2/2)$ is normalized to $\psi_e(= B_0 a^2)$. As for the helical ripple terms $\epsilon_1(\psi,\theta)$ is concerned, we chose the lowest-order polynomial for $\epsilon_h(\psi,\theta)$ and also retained only the $l\pm1$ side-band components of the helical magnetic field associated with the ripple modulation. We note that Eq.(7) is a generalized form of the σ-optimization model, $\epsilon_1 = \epsilon_h(1-\sigma\cos\theta)$, which is used for the transport optimization.[16] The modulating envelop of ripple term caused by the $l \pm 1$ side-band components

$$1 - [(\epsilon_h^{(-1)} + \epsilon_h^{(+1)})/\epsilon_h]\cos\theta$$

localizes the ripple to the inside ($\theta \sim \pi$) or the outside ($\theta \sim 0$) of the torus (see, Fig.1), depending on $\delta_h^{(-1)}, \delta_h^{(+1)} > 0$ or < 0. In the following calculation, the rotational transform $\iota(\psi)$ in Eqs.(2) and (4) is assumed to be

$$\iota(\psi) = \iota_0 + (\iota_e - \iota_0)(2\psi), \tag{11}$$

where ι_0 and ι_e are the values of $\iota(\psi)$ at the locations of magnetic axis ($\psi = 0$ or $\rho = 0$) and the plasma edge ($2\psi = 1$ or $\rho = 1$), respectively, with the definition of $\rho = r/a$. Also, we assume the electrostatic potential in the form

$$\Phi(\psi) = \Phi_0[1 - (2\psi)^\alpha]^\beta, \tag{12}$$

where α and β are the potential profile adjusting parameters.

III Effect of Electric Field on Drift Orbit Loss

We consider a $l = 2$ torsatron type device, the parameters of which are $M = 14, R_0 = 5m, a = 0.55m, \epsilon_a = 0.11, \epsilon_{ha} = 0.241, \iota_0 = 0.58$ and $\iota_e = 2.0$. It is practically important to study the drift orbits and loss regions in real space as well as velocity space from the evaluation of the device capability of the $l = 2$ low aspect ratio torsatrons. Here, we investigate the structure of loss region in a poloidal plane with toroidal angle $\phi = \pi/M$, which is shown in Fig.2. Since it has been pointed out that the electric field has a considerable influence on the high energy particle confinement as mentioned in Sec. I, we here study the effect of radial electric field on the drift orbit loss.

III-1 Orbit loss in case of $\Phi = 0$

Particle orbits possible in toroidal helical systems are classified into several types, namely, the passing, helically trapped, locally trapped and transition particles. Typical

drift orbit projected on the poloidal plane with toroidal angle $\phi = \pi/M$ (hereafter, we shall fix M = 14) are shown in Fig.3 for the case of $\Phi = 0$. For this calculation, we followed a monoenergetic particle with the kinetic energy fixed 10 KeV, and the pith angles; (a) $50°, (b)65°, (c)77.5°, (d)85°$ for typically 6 drift time ($t_{drift} \simeq a/v_d$, where v_d is the drift velocity). Particles were started from the location on given flux surface ($\rho = 0.5, \theta = 0$) or ($\rho = 0.5, \theta = \pi$), namely, outside or inside the torus. Particles shown in Figs. 3(a) - 3(d) correspond to the passing, transition, locally trapped, and helically trapped particles. The relationship between these particle orbits and the typical boundaries of loss region in velocity [17,18] as well as in real [11,12] spaces has been discussed on the basis of the theory of J-invariant.[19,20] In the present paper, however, we study in detail the loss region, by solving the guiding center drift equations (1) - (4). For these calculations, typically 2112 particles are initially distributed uniformly in the region of pitch angle 40° to 140° and in the radius $\rho = -1$ to 1 in the poloidal plane with toroidal angle $\phi = \pi/14$ (see, Fig.2). Figure 4 shows the mod - B contour map in toroidal - poloidal angle plane and the initial particle positions are also plotted by $\oplus$ sign in this fugure. We traced these particles for typically 12 drift time or until they pass through the outermost magnetic surface, where the particles are assumed to be lost. A typical result of loss region in the real space is shown in Fig. 5. The kinetic energy K = 10 KeV and no ripple modulation ($\delta_h^{(\pm 1)} = 0$) are assumed. Passing, locally trapped, helically trapped and transition particles are classified in Fig.5 by open circle ($\bigcirc$), triangle ($\triangle$), star($\star$) and lonzenge($\diamond$), respectively. The loss region is represented by the void space. The boundaries among existing regions of these particles are shown by solid lines. Thus we can easily understand what kind of particle determines the boundary of loss region. The result of loss region is in qualitative agreement with the previous results derived by J - invariant method.[12] It should be

noted that the loss region plot in real space is practically useful to evaluate two typical loss boundaries, ρ_{LLB} and ρ_{LUB}, which have been discussed in Ref.[12]. These two boundaries are plotted in Fig.5. One(ρ_{LLB}) represents the boundary of the absolute particle confinement and no particles are lost at the interior of this boundary. Another (ρ_{LLB}) gives the boundary of confined region of deeply trapped particles with $v_{\parallel} = 0$. Analytical farmula describing ρ_{LUB} will be discussed in the next section.

III-2 Orbit loss in case of $\Phi \neq 0$

We here study the effect of radial electric field E_r, on the drift orbit loss. To see how the drift orbit changes topologically under the influence of E_r, we followed a transition particle with energy fiexd 10 KeV and pitch angle 65° during 6 drift time or until they pass through the outermost magnetic surface. Particles were started from the position ($\rho = 0.5, \theta = 0$). We applied a parabolic profile for $\Phi(\psi)$, by choosing $\alpha = \beta = 1$ in Eq.(12). The variation of drift orbits projected on the poloidal plane is shown in Fig.6 when the magnitude and polarity of Φ_0 are changed; (a) $\Phi_0 = 0.0$, (b) 2 KV, (c) 4 KV, (d) – 2 KV and (e) – 4 KV. Figure 6 shows that the deviation of drift surface from magnetic surface becomes small monotonically with increasing the potential in case of $\Phi_0 > 0$ and the result becames more profound for negative potential ($\Phi_0 < 0$). To explain this situation, we note that the deviation of drift orbit is approximately given as

$$\delta \simeq v_d/(\Omega_{\nabla B} + \Omega_{E\times B}), \tag{13}$$

where v_d is the toroidal drift velocity, $\Omega_{\nabla B}$ is the poloidal precessional frequency due to ∇B - drift and $\Omega_{E\times B}$ is the poloidal rotation frequency caused by $E_r \times B$ drift. The reason that the positive potential is effective at reducing the particle orbit loss is that the radial drift of helically trapped / transition particles is reduced because the

$E_r \times B$ rotation is in the same direction as the poloidal rotation by ∇B - drift. We note that the $E_r \times B$ rotation may dominate the poloidal rotation, even at a relatively low potential level, $e\Phi_0 \simeq \epsilon_h T$ (T is the temperature). If a negative potential is created in the plasma, a resonance may occur when the $E_r \times B$ drift cancels the ∇B - drift. In this case, the particle drift changes the direction of rotation at the local resonance point, where $\Omega_{\nabla B} + \Omega_{E\times B} \simeq 0$, and the resonant supper - banana orbit is formed.[21] Examples for this type of orbit are shown in Figs. 6(b) and 6(c). If the banana width is large enough, the particle easily drifts out the plasma region (see, Fig.6(b)) because no compensation mechanism for the toroidal drift exists. Although the potential is negative, however, the further increase of the potential ($\mid \Omega_{E\times E} \mid > \mid \Omega_{\nabla B} \mid$) may reduce the banana width and consequently, the particle is again confined (see, Fig.6(c)). Thus, we expect that the large electric field can reduce effectively the particle orbit loss, regardless of its polarity. It should be noted that the role of electric field on orbit loss depends on a lot of parameters such as the particle energy, pitch ange, potential profile, and location(outside or inside the torus).

III-3 Effect of electric field on loss regions

We here study the effect of electric field on the particle confinement. In the following discussions, we assume a porabolic potential profile, $\Phi = \Phi_0(1 - 2\psi)$, by choosing $\alpha = \beta = 1$ in Eq.(12). Typical results of loss region in real space are shown in Fig.7 for the positive (A) and negative (B) potentials. The particle energy is assumed to be 10 KeV. In Fig.7(A), the boundary of loss region is represented by solid curves for (a) $\Phi_0 = 0.0$, (b) 2 KV, and (c) 4 KV. The region surrounded by dotted line denotes the existing region of locally trapped particles (see, Fig.3(c)), for the cases (a) and (b). The boundary for passing particles is indicated by dot-dash line. Figure 7(A)

shows that the loss region decreases monotonically in case of the positive potential by increasing the potential amplitude. In Fig.7(B), the boundary of loss region is shown for several values of the negative potential ; (a)$\Phi_0 = 0.0$, (b) – 2 KV, (c) – 4 KV, and (d) – 8 KV. It was found from Fig.7(B) that all trapped particles are lost due to the helical resonance in case of (b) but the further increase of the potential may reduce again the particle loss (see, (c) and (d)). For the case (c), the loss region separates the two regions at both inside and outside of the torus. With further increase of the potential, the loss region is localized only at the inside of the torus.

We next study in detail how the potential changes the spatial structure of loss region in real space. The relationship between the potential magnitude normalized to kinetic energy, Φ_0/K and the major radius normalized to plasma radius, $\rho(= r/a)$ is shown in Fig.8 for several values of pitch angle; (a) 70°, (b) 80° and (c) 90°. For these calculations, we traced the 64 × 31 particles with the energy, $K = 10KeV$ during 12 drift time or until they pass through the outermost magnetic surface. These particles were intially distributed uniformly in the region of $\Phi_0/K = -1$ to 1 and $\rho = -1$ to 1. Here, we assumed no ripple modulation, namely, $\delta_h^{(\pm 1)} = 0$. In Fig.8, the shaded region denotes the confined region and the void space represents the loss region. Also, the passing particles are shown by the dark shaded region. In the case of pitch angle 90° (see, Fig.8(c)), the loss region is localized at the outside of torus and decreases as the potential increases in the region of positive potential. On the other hand, the loss rgion spreads over the whole region if the condition for helical resonance is satisfied for a nagative potential and the loss region separates at both inside and outside of the torus in some range of negative potential. Further increase of negative potential tends to localize the loss region only inside of the torus. These results are also understandable from Figs.6 and 7. For different pitch angles (70° and 80°), the spatial structure of

loss region is topologically same except around the magnetic axis. As was shown in Fig.8(a) and 8(b), the passing particles prevent some of trapped particles from the helical resonance loss. This situation becomes notable as the pitch angle decreases from 90° to 70° because the fraction of passing particles increases as the pitch angle decreases. Moreover, we found from Fig.8 that for $\Phi_0 \simeq 0$, the loss boundary caused by helically trapped particles approarches toward the axis as the pitch angle decreases. This result is consistent with the one shown in Fig.5. We note that these results are sensitive to the potential profile. Sheared $E_r \times B$ poloidal rotation probably modify the drift orbits and resultant loss.[11] It was also pointed out that the appearance of so-called toroidal resonance may degradate the particle confinement provided that the passing particle resonates with the $E_r \times B$ rotation.[22] For the simple magnetic configuration such as no ripple modulation and for the parabolic potential profile, we can derive an analytic formular [11,12], which describes the loss boundary in case of pitch angle 90° as was shown in Fig.8(c). The analytical forms, which describe the upper and lower boundary of loss region in $\Phi_0/K - \rho$ plane, are given as

$$-\frac{e\Phi_0}{\epsilon_{ha}K} \simeq 1 - \frac{(\epsilon_{ta}/\epsilon_{ha})}{1-\rho}, \tag{14}$$

$$-\frac{e\Phi_0}{\epsilon_{ha}K} \simeq 1 + \frac{(\epsilon_{ta}/\epsilon_{ha})}{1-\rho} \tag{15}$$

where we assumed $\mu B_0 \simeq K$. When $\Phi_0 = 0$, Eq.(14) gives the loss boundary (ρ_{LUB}) for deeply trapped particles with $v_{\parallel} = 0$ in a form

$$\rho_{LUB} = 1 - \epsilon_{ta}/\epsilon_{ha}. \tag{16}$$

Taking the limit $e\Phi_0 \to \pm\infty$, ρ_{LUB} approarches the outside and inside of the plasma edge, namely, $\rho_{LUB} \to \pm 1$. The deeply trapped particles are easily confined in a configuration with small $\epsilon_{ta}/\epsilon_{ha}$ because the loss boundary and the width of loss region are sensitive to the value of $\epsilon_{ta}/\epsilon_{ha}$, which is seen from Eqs.(14)-(16).

We now study the effect of radial electric field on the minimum particle energy entering into the loss region. Typical results of the loss cone in velocity space are shown in Fig.9 for several values of the potential; $(a)\Phi_0 = 0$, (b) 1 KV, (c) 2 KV, (d) - 1 KV and (e) - 2 KV. Here we plotted the loss cone at $\rho = 0.5$ and chose the range of particle energy from 5 KeV to 20 KeV. The loss region is represented by the void space in this energy range. Figure 9 shows that the loss cone structure depends on the direction of the radial electric field. If the $E_r \times B$ rotation is in the same direction as the poloidal rotation due to the helical ripple, i.e. $\Phi_0 > 0 (E_r > 0)$ for ions, then the deviation of the drift orbit from the magnetic surface becomes small and consecuently the loss cone is reduced (see, (a), (b) and (e)). For the case of a negative potential $\Phi_0 < 0 (E_r < 0)$, however, the particle drift has a large deviation from the magnetic surface when the $E_r \times B$ rotation cancels the poloidal rotation due to ∇B, a typical drift orbit of which are shown in Fig.6(b). Loss cones associatecd with the resonant supper-banana orbit such as Fig.6(b) are shown in Figs.9(d) and 9(e). We next examine the energy dependence on the loss boundary in phase space. The results of loss region in the energy and radius$(K - \rho)$plane are shown in Fig.10 for values of the potential ; $(a)\Phi_0 = 10$ KV, (b) 0 KV and (c) - 1 KV. For simplicity, we considered only the deeply trapped particle with $v_{\|} = 0$. The confined and loss regions are represented by the shaded and void spaces, respectively. As was shown in Fig.10(b), the loss region is almost independent of the energy in the limit $\Phi_0 \to 0$. In this case, the loss boundary is given by Eq.(16). Figure 10 (a) shows the ion loss region in $K - \rho$ plane for the case of a positive potential. The minimum energy of particles entering the loss region in this case can be evaluated approximately by an analytical form[10]

$$K > K_m = \frac{e\Phi_0(1-\rho)}{\epsilon_{ta} - \epsilon_{ha}(1-\rho)} \tag{17}$$

provided $\rho > \epsilon_{ta}/\epsilon_{ha}$. Figure 10 (c) shows the case of a negative potential. In this case,

as was seen from Fig.6, the banana orbit rotates in the counter - clockwise or clockwise direction, depending on $K > e\Phi_0/\epsilon_h$ or $K < e\Phi_0/\epsilon_h$. The loss region forms a band in phase space, namely, $K_m < K < K_p$. The upper limit of the particle energy is given as

$$K_p = \frac{e\Phi_0(1-\rho)}{\epsilon_{ha}(1-\rho)-\epsilon_{ta}}, \tag{18}$$

which becomes infinite at $\rho \simeq 1 - \epsilon_{ta}/\epsilon_{ha}$ and the outside region with $\rho \geq 1\epsilon_a/\epsilon_{ha}$ is also the loss region. However, the particles with the energy less than the minimum energy, whcih is given as

$$K_m = \frac{e\Phi_0(1+\rho)}{\epsilon_{ha}(1+\rho)+\epsilon_{ta}}, \tag{19}$$

are again confined.

IV Simple Evaluation of Loss Rate Caused by Loss Cone

The loss rate in the presence of loss cone has been discussed in mirrors[23] and also in stellarators.[24]. Recently, Itoh et al. derived an approximate form, which describes the loss rate in stellarators under the influence of a loss cone in the collisionless limit.[10] Following Ref.[10], we evaluate the loss rate by employing the expression for the loss rate of deeply trapped ions,

$$\frac{1}{\tau_{loss}} \simeq \begin{cases} C\nu_i T/K_m \exp(-K_m/T), (K_m > T) \\ 2\nu_i \qquad\qquad , (K_m << T) \end{cases} \tag{20}$$

where T is the temperature, ν_i is the pitch angle seattering frequency evaluated at $K = T$, K_m is the minimum energy entering the loss cone, which is given by Eq.(17) for $E_r > 0$, and by Eq.(19) for $E_r < 0$. The coefficient C in Eq.(20) stands for the bounce averaged quantity over the magnetic surface and it is close to unity if there is a loss cone

for all poloidal angles on the magnetic surface but it becomes smaller if the loss cone is localized to a limited region of poloidal angle. Recently, a three dimensional analysis of drift orbit [2] shows that the loss region is localized at the outside of the torus ($\theta \sim 0$) at inner magnetic surfaces and it spreads towards a wide range of poloidal direction at outer magnetic surfaces. In order to evaluate C in detail, we must determine the functional dependence of θ and ρ on the coefficient C. In this paper, however, we do not consider the C-dependence and assume C=1, for simplicity. If we assume that the temperature and density profiles have the forms, $T(\rho) = T_0 f_1(\rho), n(\rho) = n_0 f_2(\rho)$, and use the notation $X_m = K_m/T$, the substitution of Eqs.(17) and (19)into Eq.(20) yields

$$\frac{1}{\tau_{loss}} \simeq \begin{cases} \nu_i / X_m exp(-X_m), (-X_m > 1), & (21a) \\ 2\nu_i \, , (X_m << 1), & (21b) \end{cases}$$

with

$$X_m = \begin{cases} \dfrac{(1-\rho)}{[\epsilon_{ta} - \epsilon_{ha}(1-\rho)]} f_1^{-1} \mid \dfrac{e\Phi_0}{T_0} \mid, (\Phi_0 > 0), & (22a) \\ \dfrac{(1+\rho)}{[\epsilon_{ta} + \epsilon_{ha}(1+\rho)]} f_1^{-1} \mid \dfrac{c\Phi_0}{T_0} \mid, (\Phi_0 < 0), & (22b) \end{cases}$$

$$\nu_i = \nu_{i0} f_2 f_1^{-1.5} \qquad (23)$$

where ν_{i0} is the pitch angle scattering frequency evaluated at $\rho = 0$. In the following discussions, we use an approximate connection formula between (21a) and (21b), which is given as

$$\frac{1}{\tau_{loss}\nu_{i0}} \simeq \frac{2}{\sqrt{1-\rho^2}} [1 + \{2X_m exp(X_m)\}^2]^{-0.5}, \qquad (24)$$

where X_m is given by Eq.(22a) for $\Phi_0 > 0$ and by Eq.(22b) for $\Phi_0 < 0$.

Typical results for the loss rate normalized to ν_{io} versus ρ are shown in Fig.11 for several values of $e\Phi_0/T_0$; $(a) e\Phi_0/T_0 = 0.01$,(b) 0.05, (c) 0.1, (d) 0.15 (solid curves),

(e) – 0.2, (f) – 0.3, and (g) – 0.4 (dotted curves). The loss rate in the region of $X_m << 1 (see, Eq.(21b))$, is also shown by broken line. Here, we assumed that $f_1(\rho) = 1 - \rho^2, f_2(\rho) = 1 - \rho^2, \Phi = \Phi_0(1 - \rho^2)$, and C = 1, for simplicity.

As was seen in Fig.8 or Fig.10, the loss region is localized at the outside of the torus for $\Phi_0 > 0$ and it is also localized at the inside of the torus provided $T < K_m$ for $\Phi_0 < 0$. The particle loss induced by these loss regions decreases as the magnitude of the potential increases regardless of its polarity. This loss cone loss reduces more rapidly in the case of $E_r > 0$ than in the case of $E_r < 0$. But, we note that these results depend sensitively on the choice of density, temperature, and potential profiles.

V Summary and Discussions

In this paper, the boundary of loss regions in real space as well as velocity space is studied in a $l = 2$ torsatron type configuration by solving the guiding center drift equations. We evaluated the loss boundary for absolute particle confinement. These results may be practically useful to evaluate qualitatively the capability of particle confinement and heating efficiency. The effects of radial electric field E_r on drift orbits and structure of loss regions were investigated in detail for the case of uniform $E_r \times B$ rotation. Although the nonuniform $E_r \times B$ rotation may affect strongly the structure of loss region,[11,12] we restricted our discussions to the case of uniform $E_r \times B$ rotation in this article. When the ion motion is considered, a positive E_r reduces a number of trapped particles and can prevent the loss of helically trapped ions through $E_r \times B$ poloidal orbit rotation. For a negative E_r, so - called helical resonance occurs when the $E_r \times B$ drift cancels the ∇B - drift, and the particles easily drift out from the core plasma region in this situation. It was confirmed that a large electric field can reduce effectively the particle orbit loss, regardless of its polarity. However, the reduction of

the loss due to this effect is expected, only when a particles kinetic energy K is on the order of or less than its potential energy, $K \leq e\Phi$. Energetic particles created by plasma heating systems have energies higher than those for which electric fields provide confinement, and these lost particles degradate the heating efficiency. From this point, we studied the relationship between the radial electric field E_r and the minimum energy K_m for deeply trapped particles entering the loss region for both positive and negative electric fields. These estimations of the minimum energy have been made for deeply trapped particles. As we can see from Fig.7 and Fig.8, however, the loss boundary determined by the transition particle is much wider, i.e., closer to the magnetic axis rather than the boundary caused by deeply trapped particles in case of $E_r > 0$. On the other hand, the severest loss boundary is determined by helically trapped particles with a smaller pitch angle in case of $E_r < 0$. Therefore, the estimated minimum energy, Eq.(17) gives an upper limit, in other words, the real minimum energy is equal to or smaller than Eq. (17) in case of $E_r > 0$. For $E_r < 0$, however, the evaluation of the minimum energy, Eq.(19) may provide a good approximation. Also, we carried out a simple evaluation of loss rate caused by the loss cone in the collisionless limit in the presence of radial electric field. We found that the loss cone loss is appreciable for a small negative electric field and decreases as the magnitude of the potential increases regardless of its polarity provided the potential is large enough. Generally, this loss cone loss reduces more rapidly for $E_r > 0$ than $E_r < 0$, when the ion motion is considered. It should be noted that the loss cone loss is sensitive to the density,temperature and potential profiles. In low density plasmas heated by electron cyclotron resonance heating, the electron temperature is often much higher than the ion temperature. Since the electron loss caused by the loss cone may increase the total loss in such plasmas, the loss cone of electrons should also be considered.

In the high density NBI heated plasmas, the negative ratial electric fields have been measured in $W7-A$[7], $H-E$[8] and CHS[9] experiments. In the low density ECH heated plasmas, the positive radial electric fields have also been measured in these experiments except for $W7-A$, where a negative field has been observed even for the ECH heated plasma. Recently, an attractive idea of high ion temperature mode operation in the so-called electron root ($E_r > 0$) is proposed associated with the design studies of LHD configuration. Since the contribution of the loss cone loss raises the temperature necessary to get a positive radial electric field, a much higher heating power is required than has been predicted by the neoclassical theory for realizing this mode operation.[10] To understand the experimental observations and to discuss the possibility of high T_i mode operation, futher extented studies are required by taking account of the effect of loss cone loss in addition to the neoclassical process.

It has been pointed out [1-3,10-12] that the inward shift of magnetic axis plays an important role on the improvement of particle confinement. The loss region can be reduced effectively by simultaneous control of vertical and quadraple fields. We here consider the effect of the harmonic components of ripple field on the loss region by using the ripple modulation model, Eq.(7). These field components are practically provided by the shift of magnetic axis, the variation of mod-B surface and the shaping of magnetic surface due to the virtical and quadrupole fields, and the pitch modulation of helical winding. For simplicity, we here retain only the $\epsilon_h^{l\pm1}$ components with $l=2$ and $M=14$ fixed. Particle loss region in real space is plotted in Fig.12 in the following three cases; $(a)\delta_h^{\pm1}=0, (b)\delta_h^{(-1)}=0.5$ and $\delta_h^{(+1)}=0.0$ and $(c)\delta_h^{(-1)}=0.8$ and $\delta_h^{(+1)}=0.0$. In this case, we assumed no electrostatic potential, $\Phi_0=0$ and other parameters are the same as in Fig.5. The result shows that the positive ripple modulation ($\delta_h^{(-1)}>0$), in other words, the inward shift of magnetic axis has a good effect on the reduction of

particle loss associated with both helically trapped and transition particles. In studying the actual configurations, the form of $\epsilon_t(\rho)$ and $\epsilon_h(\rho, \theta)$ are not always as simple as in the present paper, and the inward shift of the axis in the experiments would cause changes in the plasma radius and harmonic components of ϵ_h. Therefore, the quantitative conclusion requires the studies on the realistic inagnetic field. Recently, the effects of the magnetic axis shift on plasma characteristics are actively studied in both $H-E$[25] and CHS[26] experiments. These measurements show that the plasma stored energy depends sensitively on the position of magnetic axis. Whether the observations are correlated to the change in the magnetic shear and / or the variations of loss region, awaits further investigations.

We finally note the loss condition to determine the loss reigon. In the present paper, we assumed that the particles are lost if they reach the outermost magnetic surface. The choice of loss boundary at a position outside of the outermost magnetic surface or larger limiter radius may give a wider confined region, in other words, a narrow loss reigon, in principle. However, the particles drifting close to the surface are subject to the strong Colulomb collisions with cold electrons and / or the charge exchange loss with neutral particles.[24] We should discuss carefully the choice of loss condition to evaluate the actual boundary of loss region.

Acknowledgements

One of the authors (HS) acknowledges the useful discussions with Dr. M. Fujiwara and CHS gourp members.

References

1. J.Todoroki, T. Kaminura, H. Sanuki, T. Amano, T. Hayashi, K. Suzuki, T. Sato, K. Hanatani, M. Wakatani, and A. Iiyoshi, in Plasma Physics and Controlled Nuclear Fusion Research, 1988, Proceeding of the 12th International Conference(IAEA, Vienna, in press).

2. K. Hanatani, H.Sanuki and T. Kamimura, Bull. Jpn. Phys. Soc. (1989, October) JPS - 3p J13.

3. K. Hanatani, in the First International Toki Conference on Plasma Physics and Nuclear Fusion, December 4 - 7, 1989, Toki, Japan, III - 1, p.11.

4. H. P. Furth and M. N. Rosenbluth, in Plasma Physics and Controlled Nuclear Fusion Research, 1969, Proceeding of the Third International Conference(IAEA, Vienna) p.821.

5. H. E. Mynick and W. N. G. Hitchon, Nucl. Fusion 23, 1053(1983).

6. R. H. Fowler, J. A. Rome, and J. F. Lyon, Phys. Fluids 28, 338 (1985).

7. H. Maassberg and W7 Group, in Proc. Int. Stellarator / Heliotron Workshop (IAEA Tech. Comm. Mtg. Kyoto, 1986), Res. Rep. PPPK - 6, Vol. 1, Plasma Physics Laboratory, Kyoto Unviersity (1987) 437.

8. M. Sato and Heliotron - E Group, in Controlled Fusion and Plasma Heating (Proc. 15th Eur. Conf. Dubrovnik, 1988), Vol.12B, Part II, European Physics Sociaty (1988) 470.

9. K. Ida, S. Hidekuma and CHS Group, in the First International Toki Conference on Plasma Physics and Nuclear Fusion, December 4 - 7, 1989, Toki, Japan,

VII - 36, p.62.

10. K. Itoh, S. - I. Itoh, A. Fukuyama, and K. Hanatani, Nucl. Fusion 29, 1851 (1989).

11. K. Itoh, H. Sanuki, J. Todoroki, T. Kamimura, S. - I. Itoh, A. Fukuyama, and K. Hanatani, submitted to Phys. Fluids.

12. H. Sanuki, J. Todoroki, and T. Kamimura, submitted to Phys. Fluids.

13. W. N. G. Hitchon, Nucl. Fusion 22, 1661 (1982).

14. M. Wakatani, Nucl. Fusion 23, 817 (1983).

15. A. H. Boozer and G. Kuo - Petravic, Phys. Fluids 24, 854 (1981).

16. H. E. Mynick, T. K. Chu, and A. H. Boozer, Phys. Rev. Lett. 48, 322 (1982).

17. M. Wakatani, S. Kodama, M. Nakasuga, and K. Hanatani, Nucl. Fusion 21, 175 (1981).

18. A. Kato and M. Wakatani, J. Phys. Soc. Japan 58, 2423 (1989).

19. J. R. Cary, C. L. Hedrick and J. S. Tolliver, Phys. Fluids 31, 1586 (1988).

20. J. Tokdoroki, submitted to J. Phys. Soc. Japan.

21. K. Hanatani, F. Sano, Y. Takeiri, K. Kondo, H. Zushi, H. Okada, O. Motojima, R. Takahashi, M. Sato, S. Sudo, T. Mutoh, K. Akaishi, H. Kaneko, T. Mizuuchi, N. Noda, S. Nishimura, T. Aikiyo, A. Iiyoshi and Uo, in Proceedings of the 14th European conference on Controlled Fusion and Plasma Physics, Madrid, Spain (E.P.S., Petit - Lancy, Switzerland, 1987) Vol.11D, Part 1, p396.

22. K. Hanatani, F. - P. Penningsfeld and H. Wobig, in Proc. Int. Stellarator / Heliotron Workshop (IAEA Tech. Comm. Mtg. Kyoto, 1986), Res. Rep. PPLK - 6, Vol.1, Plasma Physics Laboratory, Kyoto University (1987) 444.

23. V. P. Pastukhov, Nucl. Fusion 14, 3 (1974).

24. K. Miyamoto, Plasma Physics for Nuclear Fusion, Iwanami, Tokyo (1976) Ch. 8 (in Japanese). K. Miyamoto, Phys. Fluids 17, 1476(1974).

25. T. Obiki, M. Wakatani, F. Sano, S. Sudo, K. Kondo, M. Sato, M. Nagasuga, H. Zushi, T. Mizuuchi, S. Besshou, H. Okada, K. Hanatani, Y. Nakamura, K. Muraoka, K. Uchino, K. Matsuo, T. Kajiwara, A. Komori, T. Yamashina, H. Minagawa, H. Matsuura, N. Noda, and H. Kaneko, in The First International Toki Conference on Plasma Physics and Nuclear Fusion, December 4-7, 1989, Toki, Japan, VI - 4, p.24.

26. S. Okamura, H. Iguchi and CHS Group, in the First International Toki Conference on Plasma Physics and Nuclear Fusion, December 4 - 7, 1989, Toki, Japan, VII-34, p.60.

Figure Captions

Fig. 1 Coordinate conventions used in the present analysis.

Fig. 2 Poloidal cross sections of the magnetic surface at $\phi = \pi/14$.

Fig. 3 Typical drift orbits projected on the poloidal plane with $\phi = \pi/14$. (a) passing particle (pitch angle 50°), (b) transition particle (65°), (c) locally trapped particle (77.5°), and (d) helically trapped particle (85°). Here, $\Phi = 0$ and K = 10 KeV are assumed.

Fig. 4 The mod - B contour map in toroidal - poloidal angle plane. The initial particle positions are also plotted by $\oplus$ mark in this figure.

Fig. 5 Loss region in pitch angle - radius $(\chi - \rho)$ plane. Here, $\Phi = 0, \delta_h^{(\pm 1)} = 0$, and K = 10 KeV are assumed. Passing, locally trapped, helically trapped and transition particles are classified by open circle (o), triangle (Δ), star($\star$) and lonzenge($\diamond$), respectively. The loss region is represented by void space. Boundaries among existing region of these particles are denoted by solid lines. ρ_{LLB} is the boundary of the absolute particle confinement and ρ_{LUB} represents the boundary of confined region of deeply trapped particles with $v_{\parallel} = 0$.

Fig. 6 Variation of drift orbits of transition particle with K = 10 KeV and pitch angle 65° under the influence of radial electric field. (a) $\Phi_0 = 0.0$, (b) 2 KV, (c) 4 KV, (d) - 2 KV and (e) - 4 KV. Drift orbits (b) and (c) correspond to resonant supper- banana orbits.

Fig. 7 Effect of electric field on loss region in real space for positive (A) and negative (B) potentials. For the case(A), (a) $\Phi_0 = 0.0$ (b) -2 KV, (c) -4 KV and (d) - 8 KV. In (A), the boundary of loss region is represented by solid curves. Existing region of locally trapped particles is shown with the surrounded region by dotted line for cases (a) and (b). Boundary for passing particles is indicated by dot - dash line. Here, K = 10 KeV and no ripple modulation, $\delta_h^{(\pm)} = 0$ are assumed. L and C denote the loss and confined regions, respectively.

Fig. 8 Spatial structure of loss region in $\Phi_0/K - \rho$ plane is plotted for several values of pitch angle ; (a) 70°, (*b*)80° and (c) 90°. The confined and loss regions in this plot are represented by shaded region and void space, respectively. Existing region of passing particles is also shown by dark shaded region. Here, K = 10 KeV and $\delta_h^{(\pm 1)} = 0$ are assumed. The boudary of loss region in case of pitch angle 90° is given approximately by Eqs.(14) and (15).

Fig. 9 Typical results of loss cone in velocity space at $\rho = 0.5$ for several values of Φ_0; (*a*)$\Phi_0 = 0.0$, (b) 1 KV, (c) 2 KV, (d) - 1 KV, and (e) - 2 KV. The loss region is represented by voide space. Here, K = 10 KeV and $\delta_h^{(\pm 1)} = 0$ are used.

Fig.10 Loss region in energy and radius $(K-\rho)$ plane for potentials ; (a) $\Phi_0 = 10KV$, (b) 0 KV and -10 KV in case of deeply trapped particles with $v_{\|} = 0$. The confined and loss regions are represented by the shaded region and void space, respectively. Boundaries of loss region are given approximately by analytical expressions, Eq.(17) in (a), Eq.(16) in (b) and Eq.(18) and Eq.(19) in (c).

Fig.11 Loss rate normalized to ν_{i0} versus ρ, where ν_{i0} is the pitch angle scattering frequency evaluated at $\rho = 0$, are plotted for typical values of the potential energy normalized to the temperature T_0 at $\rho = 0$. Here, (a) $e\Phi_0/T_0 = 0.01$, (b) 0.05, (c) 0.1, (d) 0.15 (solid curves), (e) - 0.1, (f) – 0.3 and (g) – 0.4 (dotted curves). Loss rate in the case of $K_m/T << 1$, where K_m is the minimum energy entering the loss cone and $K \simeq T$ is the particle kinetic energy.

Fig.12 Effect of ripple modulation on loss region in real space for three cases; (a) $\delta_h^{(\pm)} = 0$, $(b)\delta_h^{(-1)} = 0.5$ and $\delta_h^{(+1)} = 0$, and (c) $\delta_h^{(-1)} = 0.8$ and $\delta_h^{(+1)} = 0$. Here, K = 10 KeV and $\Phi_0 = 0$ are used. L and C denote the loss and confined regions, respectively.

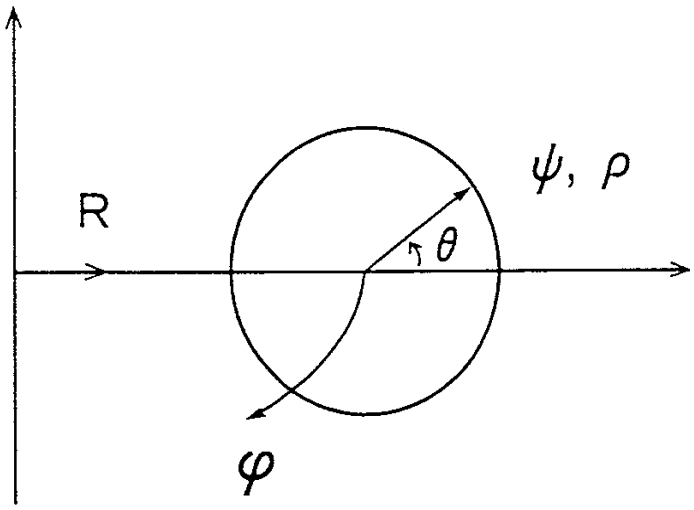

Fig.1

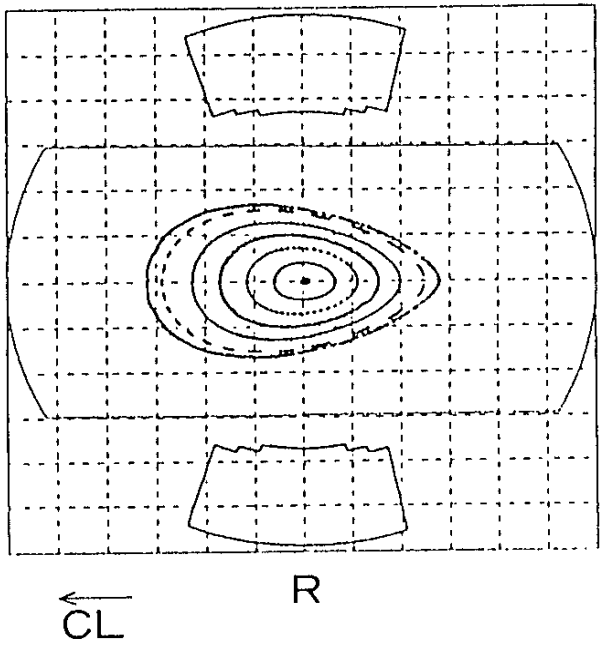

Fig.2

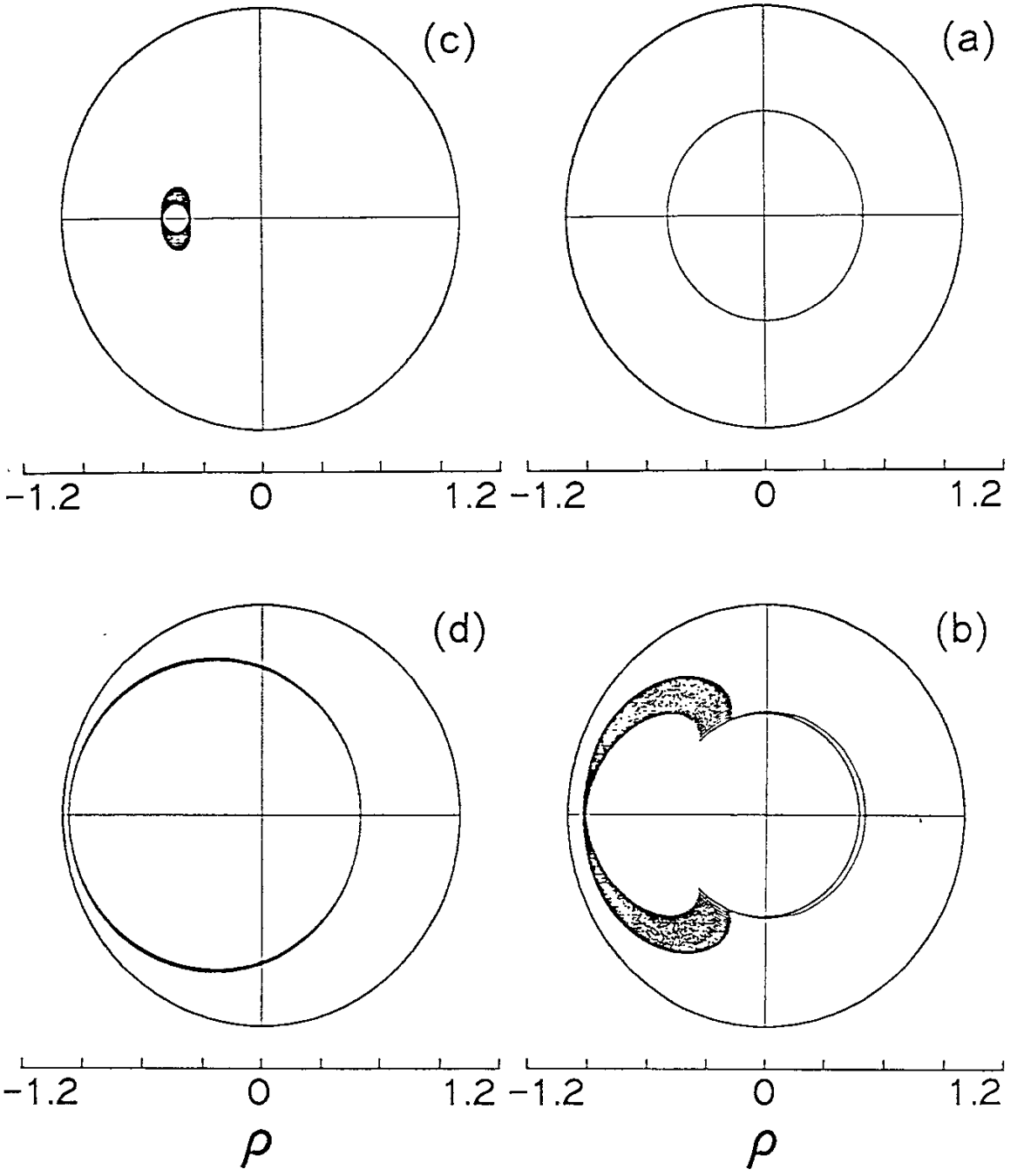

Fig.3

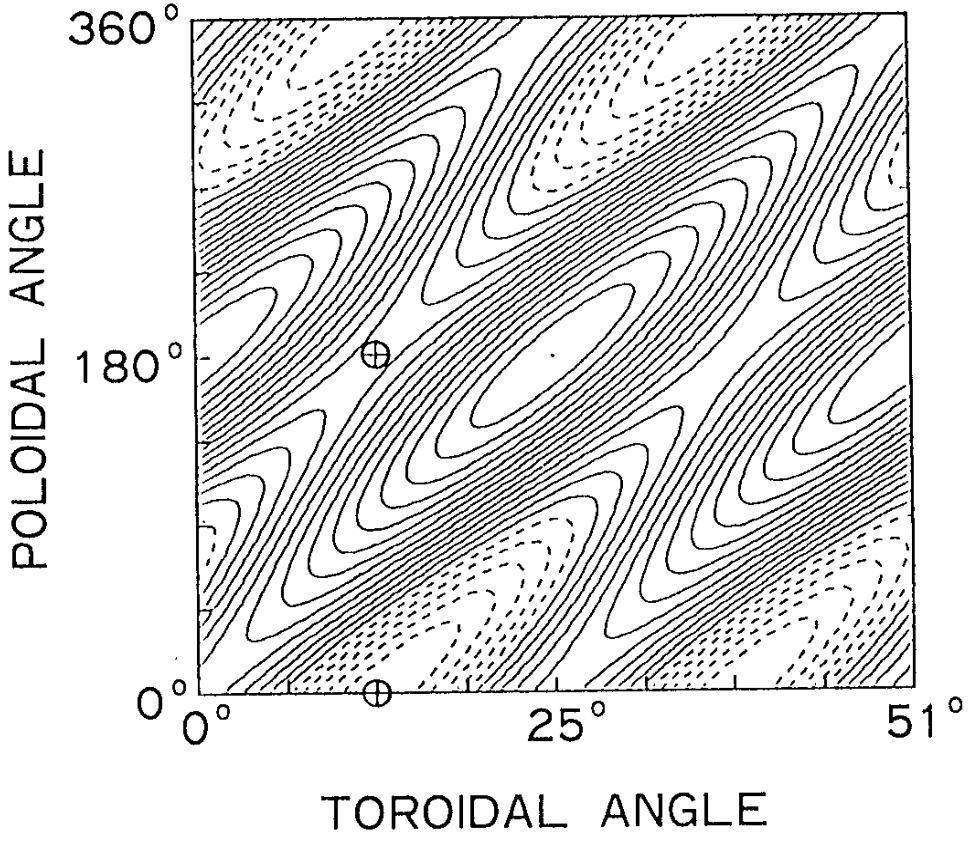

Fig.4

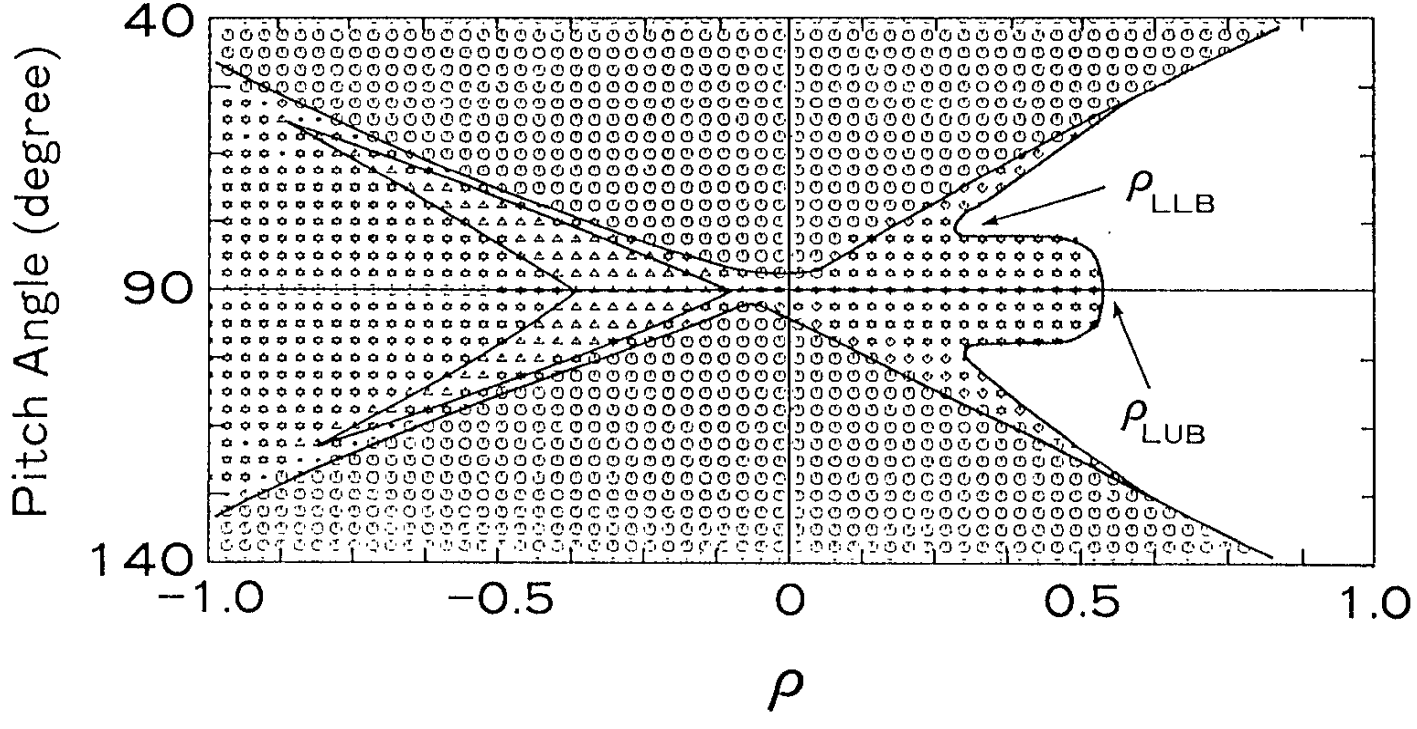

Fig.5

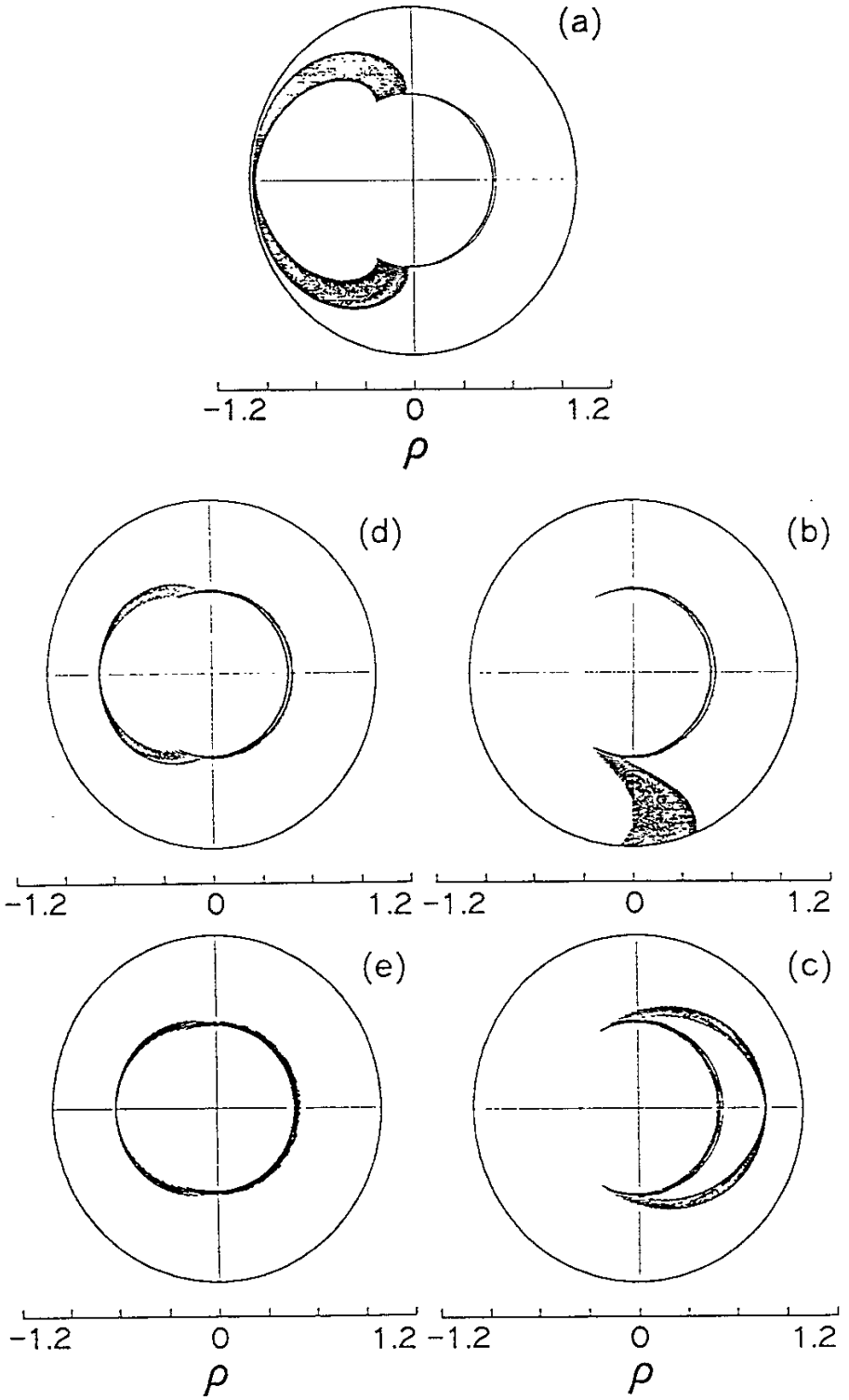

Fig.6

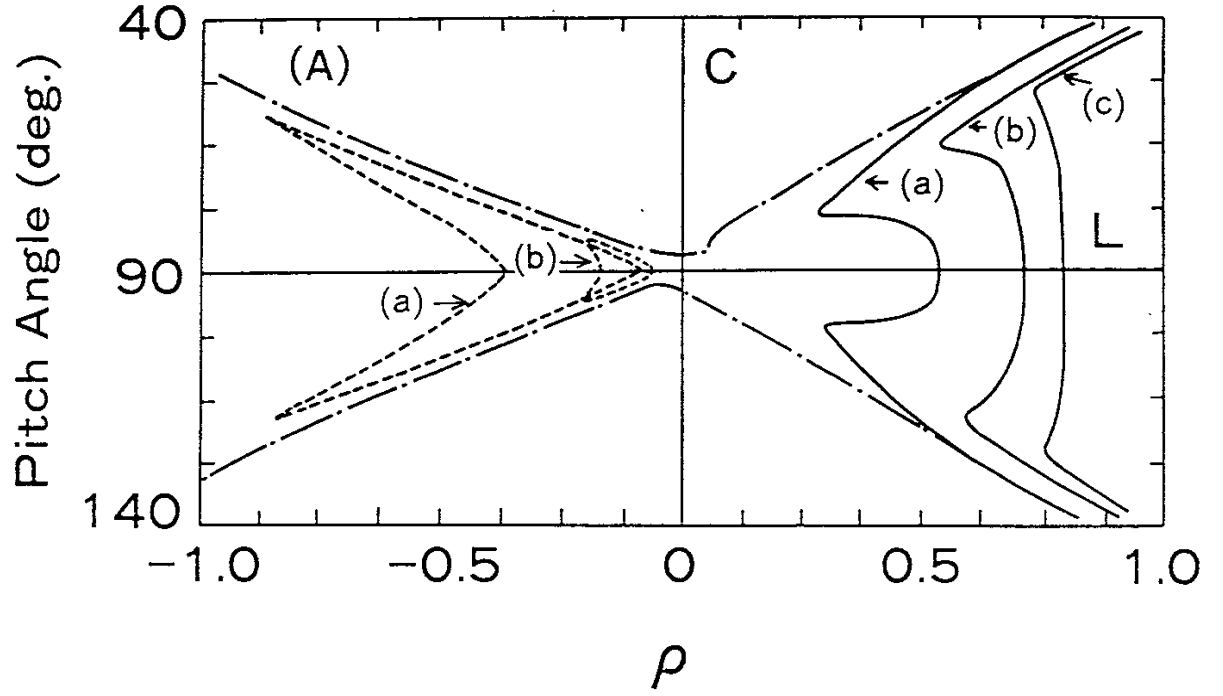
40
90
140
Pitch Angle (deg.)
(A)
C
(a)
(b)
(c)
L
−1.0
−0.5
0
0.5
1.0
ρ

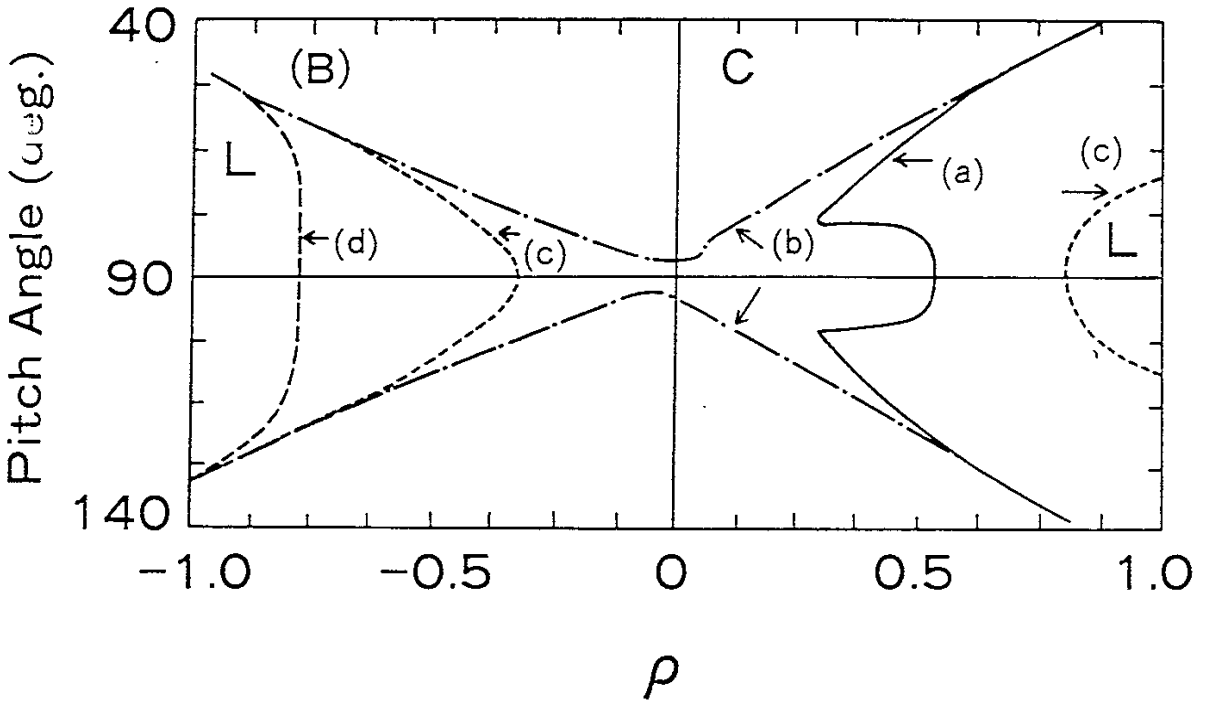
40
90
140
Pitch Angle (deg.)
(B)
C
L
(a)
(b)
(c)
(d)
L
−1.0
−0.5
0
0.5
1.0
ρ

Fig.7

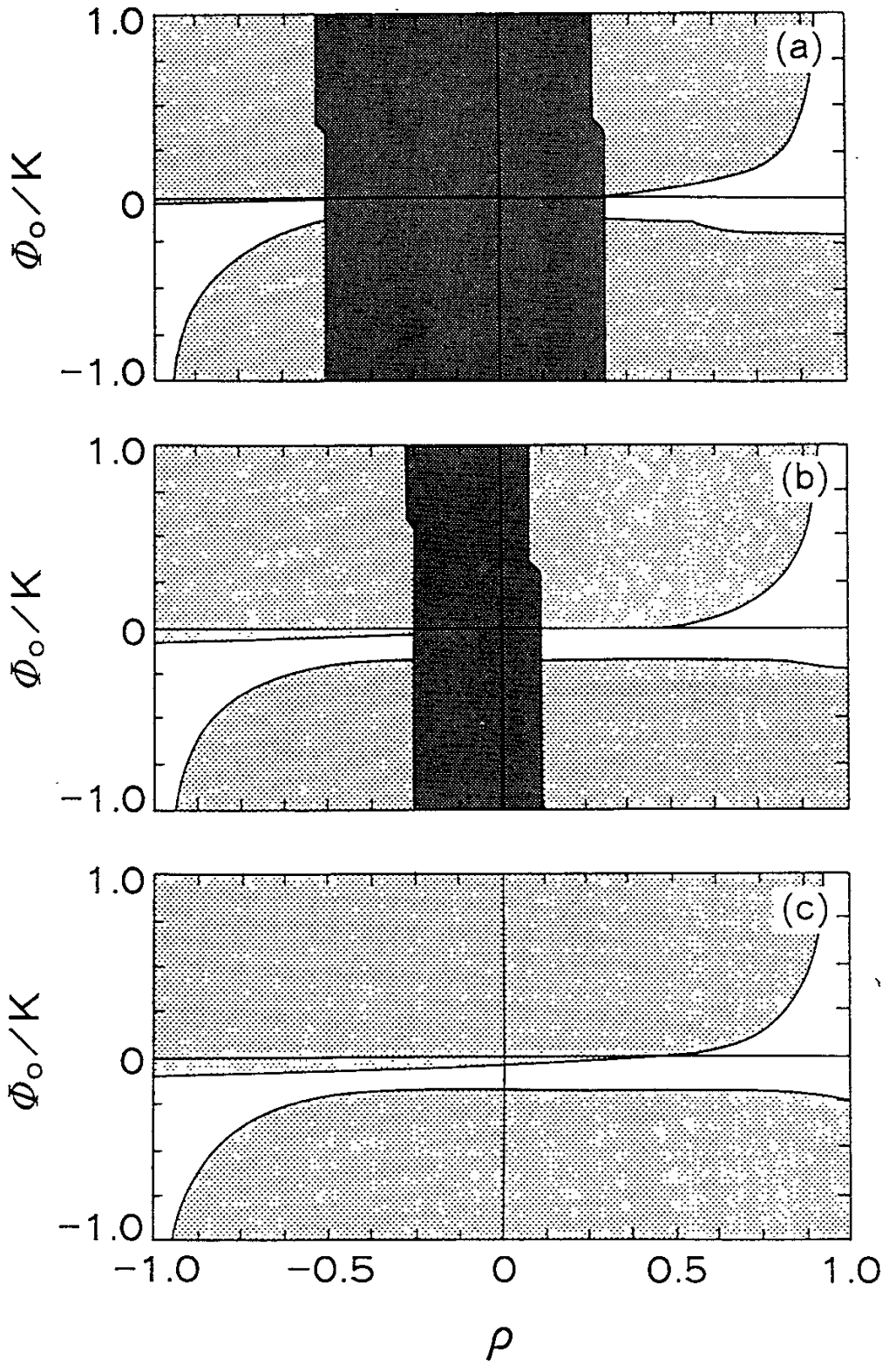

Fig.8

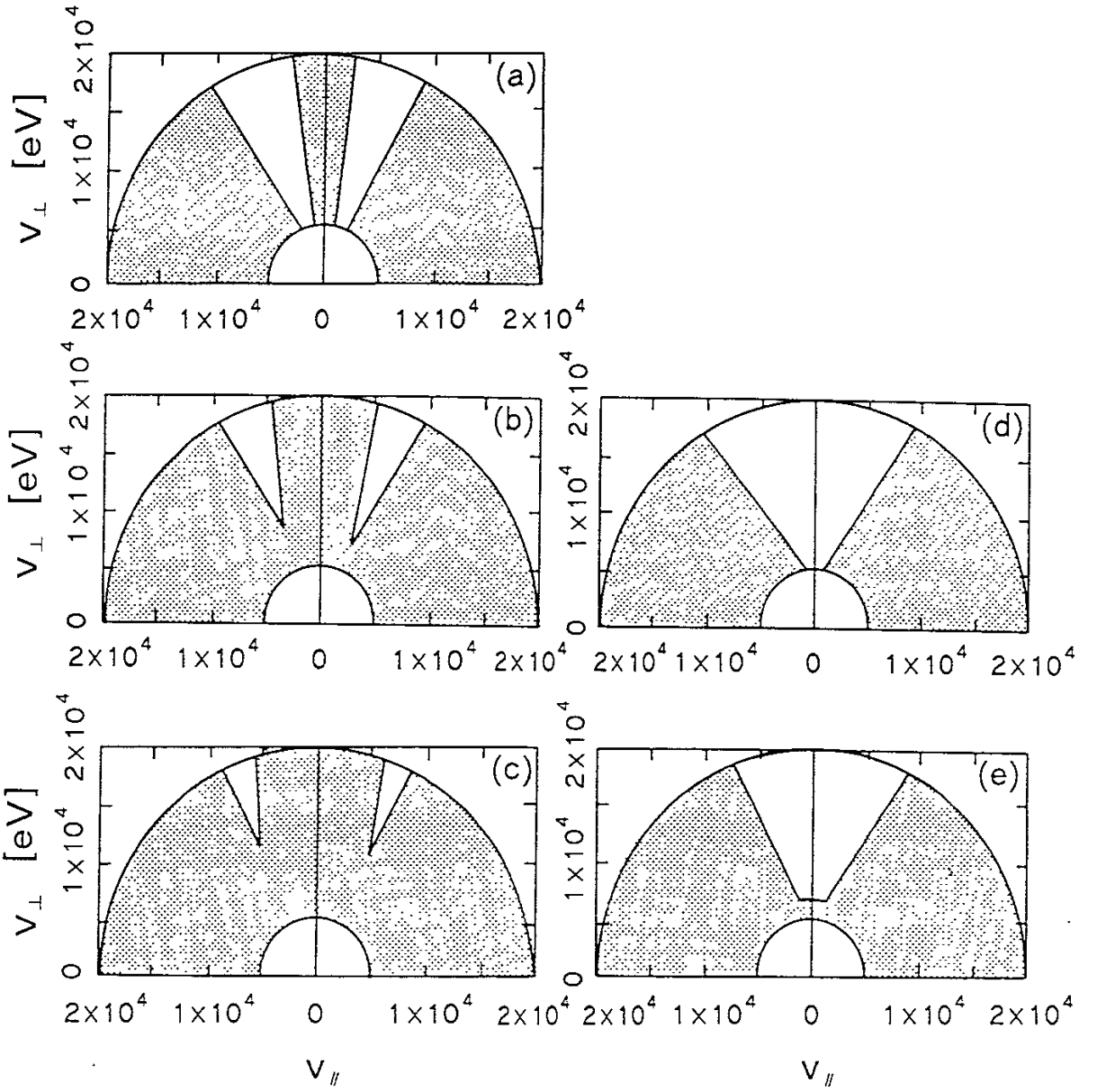

Fig.9

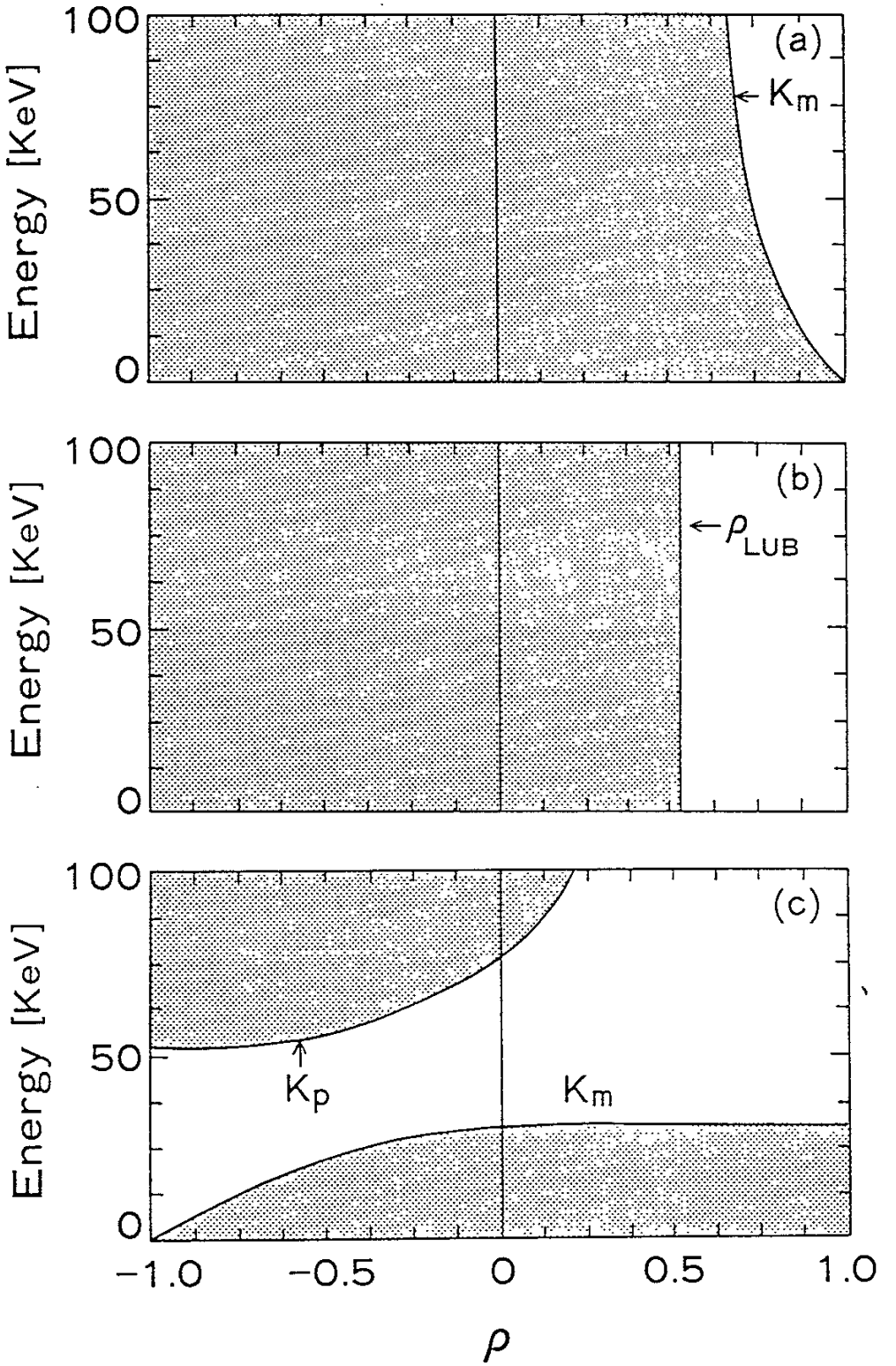

Fig.10

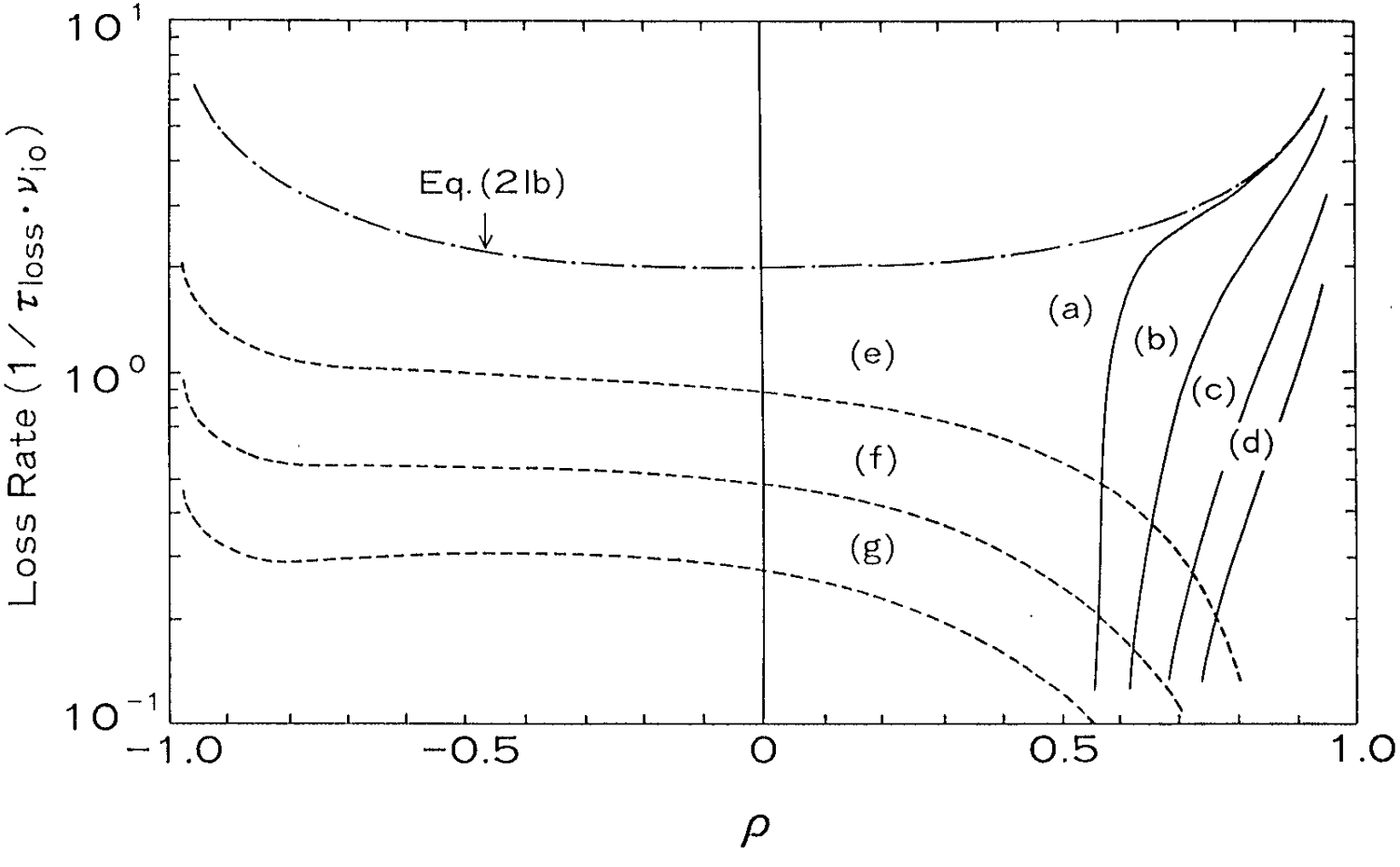
10^1
10^0
10^{-1}
Loss Rate $(1/\tau_{loss}\cdot\nu_{io})$
Eq. (21b)
(a)
(b)
(c)
(d)
(e)
(f)
(g)
−1.0
−0.5
0
0.5
1.0
ρ

Fig.11

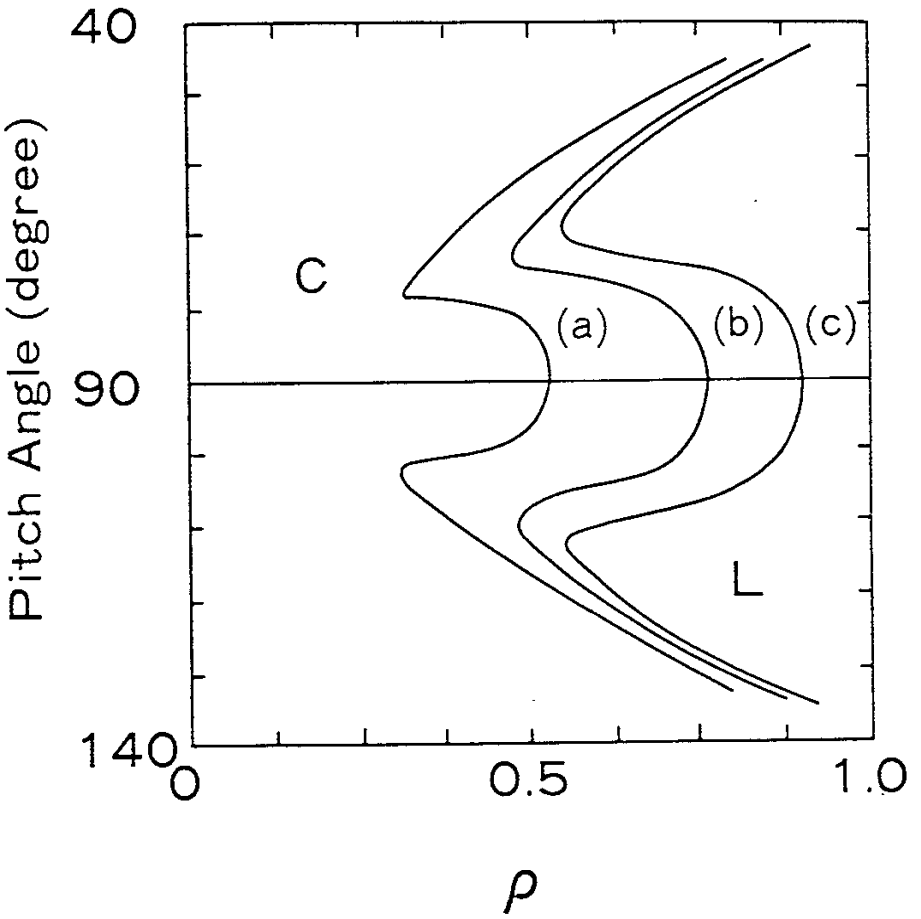

Fig.12